Journal of
Ceramic Science
and Technology

J. Ceram. Sci. Technol., **12** [2] 81-86 (2021)
DOI: 10.4416/JCST2020-00023
available online at: http://www.ceramic-science.com

Influence of Different Zn Substitution Sites on the Crystallinity and Morphology of Zn-Doped Nano-Hydroxyapatite Powder

Yangyang Wang*[1], Tao Wang[1]

[1]College of Materials Science and Technology, Nanjing University of Aeronautics and Astronautics, Yudao Street 29, Nanjing 210016, China

received October 16, 2020; received in revised form February 17, 2021; accepted March 16, 2021

Abstract

Zn-substituted hydroxyapatite (ZnHA) has been studied as a biomaterial with enhanced biological activity, which is related to its crystal structure and micromorphology. We investigated the inner contacts at the sites of Zn-substitution, crystal structure conversion behavior and variation of morphology in ZnHA. The composition of samples with different Zn/(Zn+Ca) molar ratios (0 mol%, 1 mol%, 5 mol%, 10 mol% and 20 mol%) was characterized by means of X-ray diffraction (XRD) and Fourier-transform infrared spectroscopy (FTIR). The morphologies of samples were examined with scanning electron microscopy (SEM) and high-resolution transmission electron microscopy (HRTEM). The Zn^{2+} ion distribution was analyzed by means of X-ray photoelectron spectroscopy (XPS). From the XRD and FTIR data, it could be observed that the crystallinity of the precipitates decreased with increasing content of Zn^{2+} ions, with the formation of amorphous phase when the concentration of Zn^{2+} ions exceeded 10 mol%. SEM and HRTEM results showed that the morphologies changed from nano-needle clusters to nanospheres with increasing concentration of Zn^{2+} ions. According to the XPS results, at low Zn concentrations (0 – 5 mol% Zn), the Zn^{2+} ions only occupied the Ca(II) sites. However, with the increase in the concentration of Zn^{2+} ions, Zn^{2+} ions also gradually occupied the Ca(I) sites. Hence, we can conclude that the change in morphology and crystal structure is affected by the Zn^{2+} ions occupying the different Ca^{2+} ions sites.

Keywords: Zn-doped, hydroxyapatite, morphology, crystal structure, substituted sites

I. Introduction

Hydroxyapatite (HA, $Ca_{10}(PO_4)_6(OH)_2$) is the main inorganic component in human bones and tooth enamel. It has been widely used for repairing and replacing damaged parts of human bones owing to its osteoconductive property, bioactivity, lack of irritation, chemical stability and biocompatibility [1–3]. As a consequence, it is a well-known bioceramic material.

To study the effects of different elements on the properties of HA, several ionic substitutions (Fe^{3+}, Mg^{2+}, Zn^{2+}, Sr^{2+}, CO_3^{2-}) have been made in pure HA [4–8]. Zn has been proven to enhance the biological activity of HA as a trace element [9]. The concentration of Zn in human bone is 125 – 250 ppm [10]. According to Yuan's study, the ability of bone marrow mesenchymal stem cells (MSCs) to differentiate into osteoblasts is quite sensitive to the physical composition and chemical properties of materials [11]. Zn-doped apatite with a special composition and crystal structure can promote the formation of new bone by increasing the growth rate of the osteoblasts and can also stimulate collagen production [12, 13]. Moreover, these properties are affected by the different crystallinity and morphology of Zn-doped HA [14, 15].

Zn^{2+} (0.074 nm) has a similar ion radius to that of Ca^{2+} (0.1 nm) and can replace Ca^{2+} in HA [16]. Different techniques have been used to synthesize Zn-substituted HA, e.g. electrochemical [17], microwave irradiation [18], plasma spray [19], aqueous precipitation [20], and sol-gel techniques [21]. Owing to the simplicity, controllability and product stability, aqueous precipitation is one of the easiest methods to prepare Zn-substituted HA.

The structure and properties of Zn-doped HA have been previously studied based on Density Function Theory (DFT) calculations [22, 23]. Based on these studies, Ca(I) and Ca(II) sites are the two kinds of Ca^{2+} sites in a HA lattice. In a Ca(I) site, Ca^{2+} ions coordinate with nine oxygen atoms to form a Ca_1O_9 polyhedron. In a Ca(II) site, Ca^{2+} ions coordinate with six oxygen atoms and one hydroxyl group to form a Ca_1O_7 polyhedron. However, the influence of Zn occupying different Ca sites on the morphology and crystal structure conversion of ZnHA has been analyzed less with experimental methods.

In the present study, the morphology and crystal structure have been analyzed by means of XRD, FTIR, SEM, and HRTEM. In our work, we have used the XPS method to analyze the Zn^{2+} substituted sites. XPS has been used for the first time as an experimental method in the analysis of Zn^{2+} substitution. Here, we demonstrate that the morphology and crystal structure of ZnHA change when Zn^{2+} ions occupy different Ca^{2+} ions sites with increasing Zn^{2+} content.

* Corresponding author: yywang8712@nuaa.edu.cn

II. Experimental

(1) Preparation of Zn-substituted HA powder

Stoichiometric ZnHA [(Ca+Zn)/P=1.67] powders were synthesized by means of aqueous precipitation with different Zn/(Zn+Ca) molar ratios. All the chemical reagents used in the preparation of ZnHA samples, including zinc nitrate ($Zn(NO_3)_2$), calcium nitrate ($Ca(NO_3)_2$) and diammonium hydrogen phosphate ($(NH_4)_2HPO_4$) were analytically pure. $Zn(NO_3)_2$ and $Ca(NO_3)_2$ were dissolved in deionized water to prepare the 0.5 M-Ca-/Zn-containing solution, while the pH was adjusted to 10 with ammonia solution. Then this mixed solution was poured into a round-bottom flask. In the next step, 500 ml of 0.3 M $(NH_4)_2HPO_4$ solution was added slowly into the above-mentioned mixed solution, the pH was kept at 10 by the ammonia solution, and the mixed solution heated at 60 °C for 2 h in a water-bath bed while being constantly stirred with a Teflon stirring bar. Next, the mixed solution was kept at room temperature for 48 hours for aging. After aging, the product was filtered and washed repeatedly with deionized water until neutral. Finally, the product was freeze-dried to obtain dry powders in a vacuum freeze dryer. Zn-substituted HA powders were prepared with different Zn/(Zn+Ca) molar ratios, i.e. 0 mol%, 1 mol%, 5 mol%, 10 mol% and 20 mol%, the synthesized powders were labeled HA, Zn1-HA, Zn5-HA Zn10-HA and Zn20-HA, respectively.

(2) Material characterization

The phase crystallinity of the synthetic samples was characterized by means of X-ray diffraction (XRD, Bruker D8) using CuKα (40 mA, 40 kV). The 2θ range is from 10° to 80° with a scanning speed of 2.0° (2θ)/min.

The chemical composition of the synthetic samples was examined by means of Fourier transform infrared spectroscopy (FTIR, NEXU670) with the transmittance mode. The standard KBr pellet technique was employed. The measurements were recorded 64 times for the spectral range of 400 – 4 000 cm^{-1}.

A field-emission scanning electron microscope (FESEM, FEI Quanta 200) was used to analyze the morphology of the synthetic samples. The powders were suspended in ethyl alcohol with the ultrasonic method, and then deposited on an aluminum wafer. Owing to the poor conductivity of ZnHA, it must be coated with gold to increase its conductivity and to obtain higher image resolution. Thus, the surface of the samples was coated with a gold layer by means of a gold-spraying instrument (108 Auto/SE).

The detailed morphologies of the synthetic samples were observed with a high-resolution transmission electron microscopy (HRTEM, FEI Tecnai 20). The crystallinity of the samples was analyzed by means of selected area electron diffraction (SAED).

The elemental composition of the synthetic powders and the atomic binding energy were characterized by means of X-ray photoelectron spectroscopy (XPS, PHI5000) with monochromatic AlKα (1486.7 eV) radiation (15 kV, 25 W) and a beam size measuring 100 μm in diameter.

III. Results and Discussion

(1) Material composition

Fig. 1 shows the XRD patterns of the synthetic ZnHA with various Zn^{2+} ion concentrations. Within the compositions, the intensity of the XRD peaks widened, indicating that the crystallinity of the synthesized ZnHA significantly decreased with increasing concentration of the Zn^{2+} ions. For the HA, Zn1-HA and Zn5-HA samples, diffraction peaks at 2θ = 25.8° and 31.9° were consistent with the characteristic diffraction peaks of pure hydroxyapatite (JCPDS #00 – 009 – 0432) and kept the hexagonal crystal structure. No other significant peaks were detected.

The lattice parameters (a, c) of synthesized samples are shown in Table 1; they have been calculated with MDI Jade 6.5 software. The crystallite size was estimated with Scherrer's equation. Compared to pure HA, the values of the lattice parameters (a, c) decreased when Zn^{2+} ions substituted Ca^{2+} ions in the HA lattice. This is because the ionic radius of Zn^{2+} is smaller than that of Ca^{2+}. When Zn^{2+} substituted Ca^{2+}, the cell volume became smaller. In addition, the crystallinity of ZnHA also decreased with the increase in the Zn^{2+} ion concentration. As the concentration of Zn^{2+} ions increased above 10 mol%, the amorphous phase appeared with a characteristic halo from 25.0° to 35.0°, which was consistent with an earlier study of amorphous calcium phosphate (ACP) [24]. That is because the crystal structure of ZnHA changed from long-range order

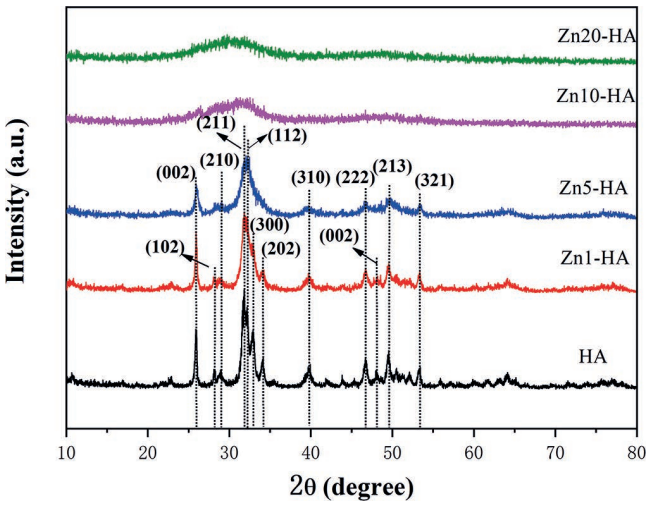

Fig. 1: XRD patterns of HA with various Zn^{2+} ions concentrations.

Table 1: Effects of Zn-substituted concentration on the ZnHA lattice parameters.

Sample	a(nm)	c(nm)	Crystallinity (%)
HA	9.4116	6.8706	95
Zn1-HA	9.4101	6.8609	90
Zn5-HA	9.3777	6.8579	55

to disorder without consistent crystal orientation. Thus, no obvious diffraction peak can be detected with XRD. Therefore, those lattices parameters could not be calculated when the Zn^{2+} ion concentration exceeded 10 mol%. This implies that Zn^{2+} ions can stabilize the amorphous calcium phosphate phase in aqueous solution in these conditions.

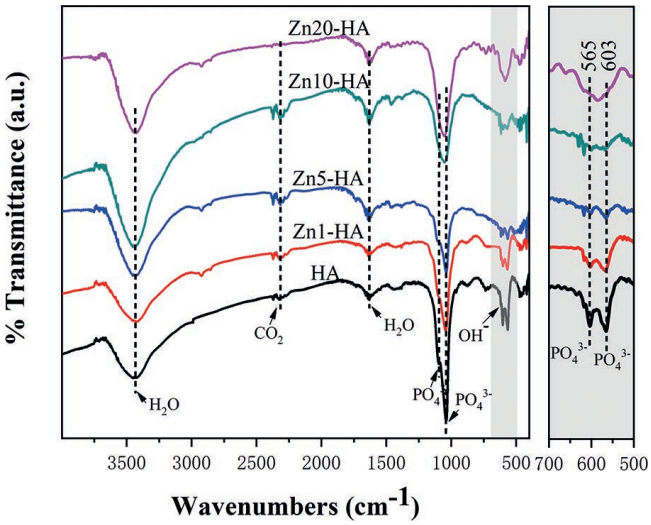

Fig. 2: FTIR spectra of the synthetic ZnHA samples with different Zn-substituted concentrations.

Fig. 2 shows the FTIR spectra of the synthetic ZnHA samples with various Zn^{2+} ion concentrations. The broad bands at 2 800 – 3 600 cm^{-1} and 1 631 cm^{-1} were ascribed to absorbed water. The band at 2 325 cm^{-1} was associated with the absorbed carbon that may come from the carbon dioxide in the air. The bands at around 603, 725, 1039 and 1 093 cm^{-1} were related to the different vibrational modes of the phosphate groups. With increasing Zn^{2+} ion concentration, the distinction between two PO_4^{3-} stretching peaks (565 and 603 cm^{-1}) became obscure and they gradually changed into a single peak, which was caused by the different local electrical field between the amorphous and crystalline phase [25]. It suggests that the crystallinity of the HA has decreased and the ACP phase has formed with increasing Zn^{2+} fraction, which agrees with the XRD results.

(2) Morphology and crystallinity

Fig. 3 shows the size and morphologies of the synthetic ZnHA samples. As shown in Fig. 3(a), the nano-needle particles were pure HA, with a length ranging from 100 – 200 nm and width of about 20 nm. As the Zn^{2+} ion concentration increased, the morphologies changed to nanospheres with diameters around 50 – 100 nm, which were inclined to agglomerate, as illustrated in Fig. 3(d). Like the results above, this indicates that the size and morphologies of the ZnHA were affected by the Zn^{2+} ion doping content.

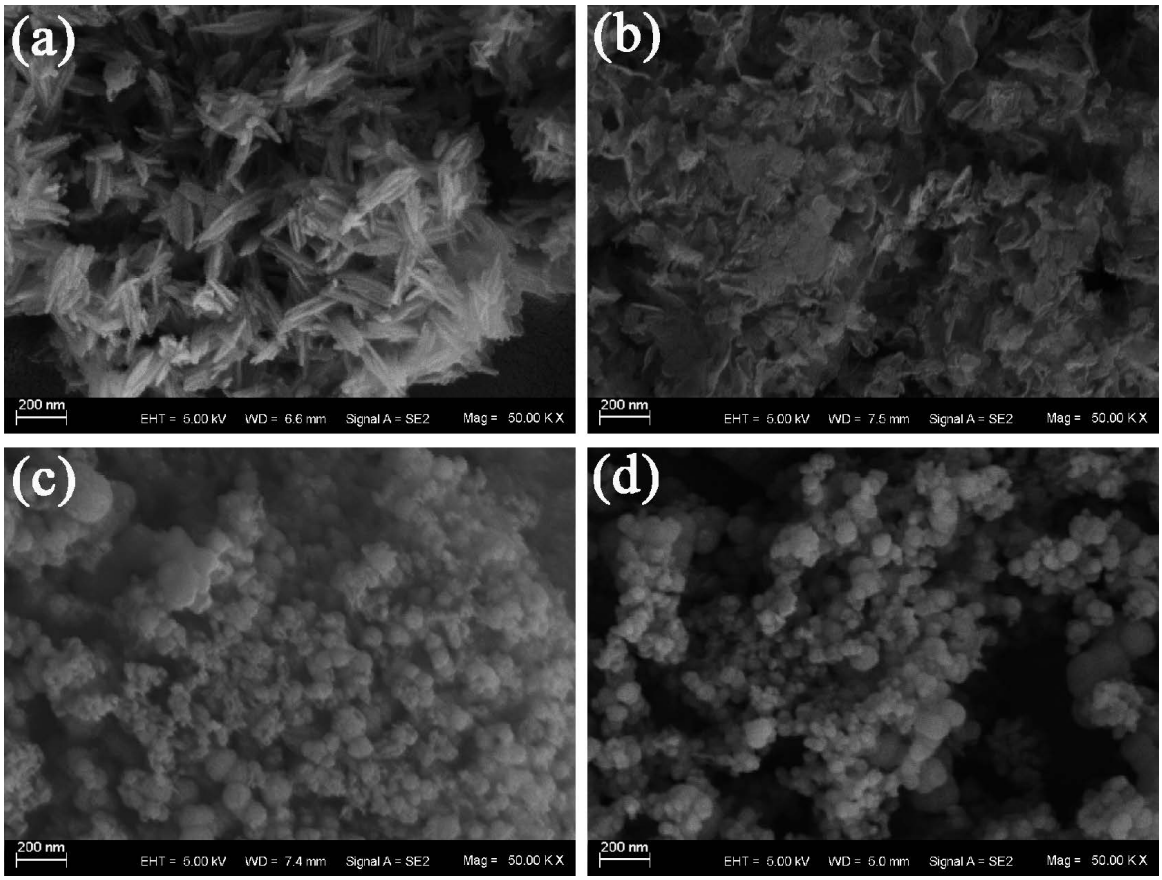

Fig. 3: SEM micrographs illustrating typical particle morphology of pure and Zn-substituted HA samples (a) HA, (b) Zn5-HA, (c) Zn10-HA, (d) Zn20-HA.

The detailed morphologies and crystallinity of the synthetic ZnHA were investigated by means of HRTEM and SAED. It could be observed that the morphologies of the ZnHA particles changed from nano-needle particles to nanosphere agglomerations with increasing Zn^{2+} content. In Fig. 4(a), the size of HA nano-needle particles was about 25 nm in diameter and 150 nm in length. The size of the particles decreased, and those particles were inclined to agglomerate significantly as the Zn^{2+} concentration increased. The particles changed to nanospheres with diameters measuring around 50 – 100 nm, as illustrated in Fig. 3(d). These HRTEM examinations of HA nanospheres were consistent with the results of the SEM observation. It implies that Zn^{2+} ions can affect the nucleation and growth of HA in liquid, a similar finding to that in Kumar's study [26]. The crystallinity of these samples was further revealed by SAED patterns (Fig. 4, inserts). As shown in Fig. 4(c), the observation of a halo diffraction ring indicated the formation of amorphous phase. According to the diffraction pattern, the crystallinity of the HA decreased significantly with increasing Zn^{2+} ion concentration.

During the transformation of ACP to HA, the substitution of Zn^{2+} ions for Ca^{2+} ions obstructed the atomic rearrangement in HA lattice. Thus, amorphous ZnHA was kept stable in aqueous solution.

The produced phases changed from crystalline HA to ACP with the increasing fraction of Zn^{2+} ions. As deduced from the combination with XRD data, Zn^{2+} ions inhibited the growth of the apatite crystals in a-axis and c-axis direction. In aqueous media, ACP is formed first. Then it is spontaneously converted to other calcium orthophosphates. In the next step, the calcium orthophosphates act as seeds or templates to facilitate apatite nucleation and crystal growth. Finally, the HA is formed. For pure HA, the crystal grows along the preferred direction. Thus, it achieves needle-like morphology. For ZnHA, the nucleation process of the calcium orthophosphates needs to overcome the lattice distortion energy caused by the different ionic radius between Zn^{2+} and Ca^{2+}. So, the ACP phase is preserved without any preferred direction. Finally, it achieves nanosphere morphology. Therefore, the morphologies changed from needle-like particles to nanospheres.

(3) Zn^{2+} ion distribution

Fig. 5 presents the XPS general spectrum of ZnHA samples with different Zn^{2+} ion concentrations. The peak for phosphorus (P 2p, P 2s), oxygen (O 1s) and calcium (Ca 2p, Ca 2s) could be observed in Zn-substituted HA. On the other hand, the major peak assigned to Zn 2p1 and Zn 2p3 was observed at a binding energy value of around 1044 eV and 1022 eV, in agreement with the findings reported by Moulder [27]. With the addition of Zn^{2+} ions, the Zn 2p1 and Zn 2p3 peaks increased, whereas the Ca 2p and Ca 2s peaks decreased. These results suggest that the synthesized samples were Zn-substituted hydroxyapatite, demonstrating that the Zn^{2+} ions were structurally incorporated into the HA lattice in the place of Ca^{2+} ions with increasing Zn^{2+} ion content.

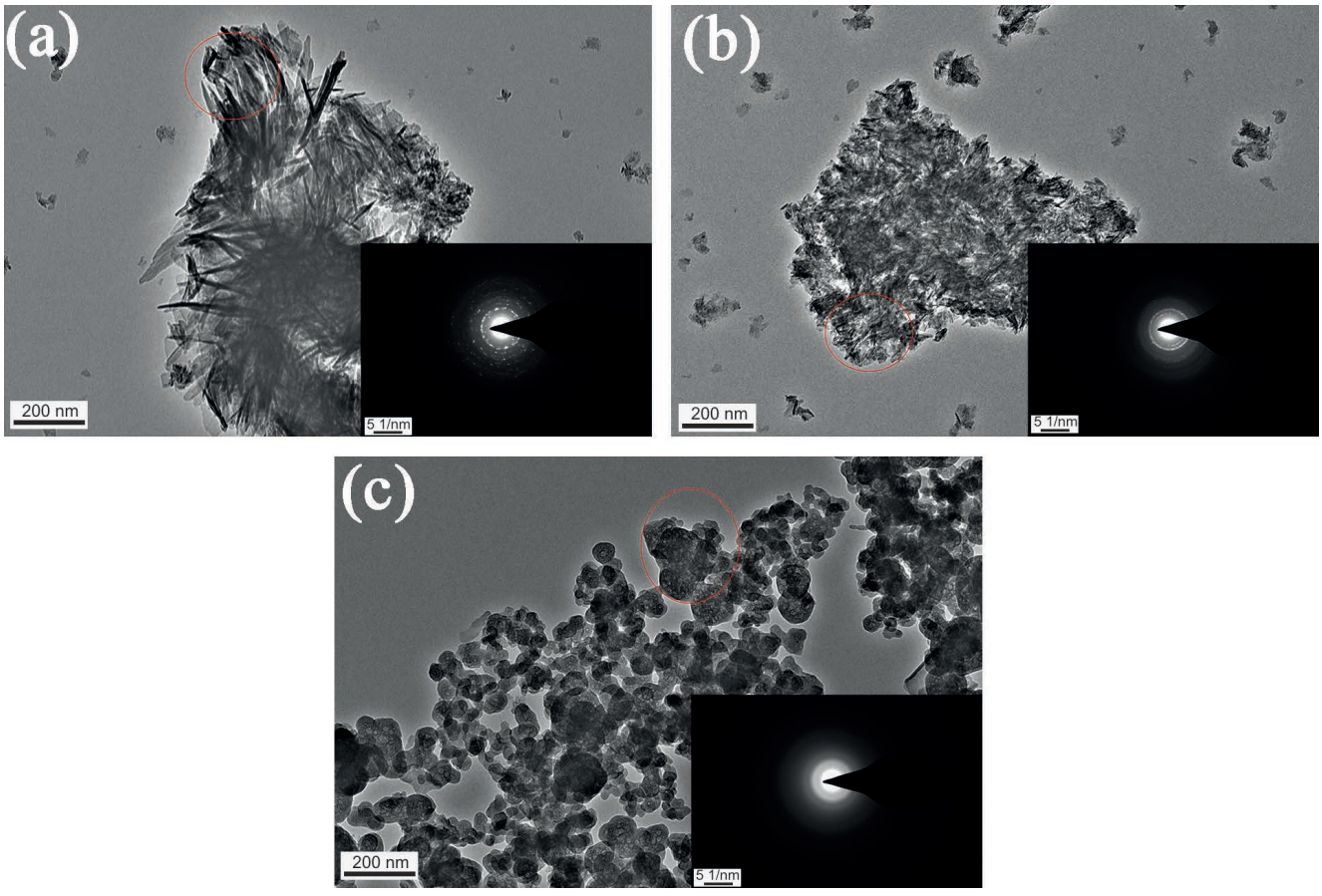

Fig. 4: TEM images and the corresponding SAED patterns of the ZnHA samples (a) HA, (b) Zn5-HA, (c) Zn10-HA.

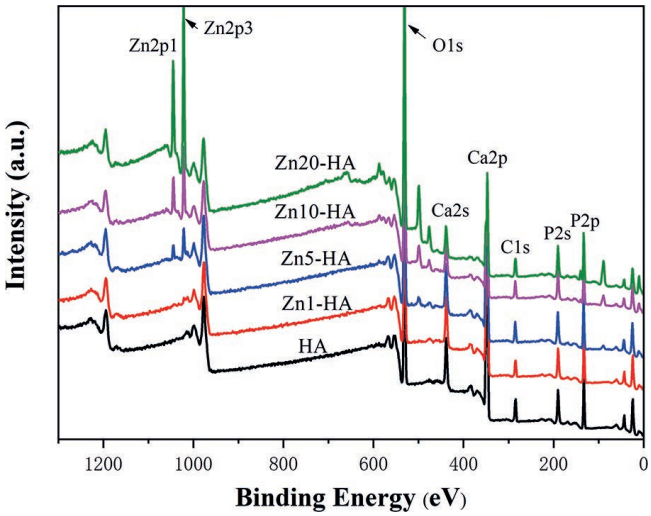

Fig. 5: X-ray photoelectron general spectrum of ZnHA samples.

Fig. 6 depicts the separated spectral fitting data of the Zn 2p peak in the total XPS spectra of ZnHA with different Zn^{2+} concentrations. Based on previous research, Ca(I) and Ca(II) sites are the two kinds of Ca^{2+} sites in HA lattice [28]. Ca(I) ions coordinate with nine oxygen atoms to form a Ca_1O_9 polyhedron. Ca(II) ions coordinate with six oxygen atoms and one hydroxyl group to form a Ca_1O_7 polyhedron. According to the study by Guo, the binding energy of Sr^{2+} ions occupying Ca(I) and Ca(II) sites can be divided into two different peaks [29]. Thus, combined with the separated spectral, the lower peaks (1021.66, 1044.80 eV) and higher peaks (1022.66, 1045.78 eV) were related to the atomic binding state of Zn^{2+} ions occupying the Ca(II) sites and Ca(I) sites, respectively. At low Zn concentrations (0 – 5 mol% Zn), the Zn^{2+} ions only occupied the Ca(II) sites. However, when the Zn content exceeded 10 mol%, one partial Zn^{2+} ion occupied the Ca(I) sites. Moreover, at high Zn concentrations (10 – 20 mol% Zn), the Zn^{2+} ions occupied both Ca(II) sites and Ca(I) sites. As analyzed above, the separated fitting data of Zn 2p can be used to analyze the occupying sites of Zn^{2+} in a HA lattice.

In combination with these analyses above, the crystal structure and morphology of ZnHA are related to the Zn^{2+} ions occupying different Ca sites. As the Zn^{2+} ion concentration increases, the degree of crystallinity in the ZnHA decreases. When the Zn^{2+} concentration is below 5 mol%, Zn^{2+} ions occupy merely Ca(II) sites of the HA lattice. ZnHA maintains a similar crystal structure and nano-needle morphology to that of pure HA. When the Zn concentration is above 10 mol%, Zn^{2+} ions occupy both Ca(I) and Ca(II) sites. Moreover, as the content of Zn^{2+} increases, the Zn^{2+} ion occupying ratio of Ca(I) sites to Ca(II) sites increases. The amorphous phase appears and the morphology of HA changes from needle-like particles to nanospheres. These results show that the process of Zn^{2+} ions occupying the Ca(I) sites promotes the formation of amorphous phase and the change in morphology. Zn^{2+} ions occupy Ca(I) sites preferentially. As a result, we can speculate that Zn^{2+} ions occupying Ca(I) sites play the leading role in the

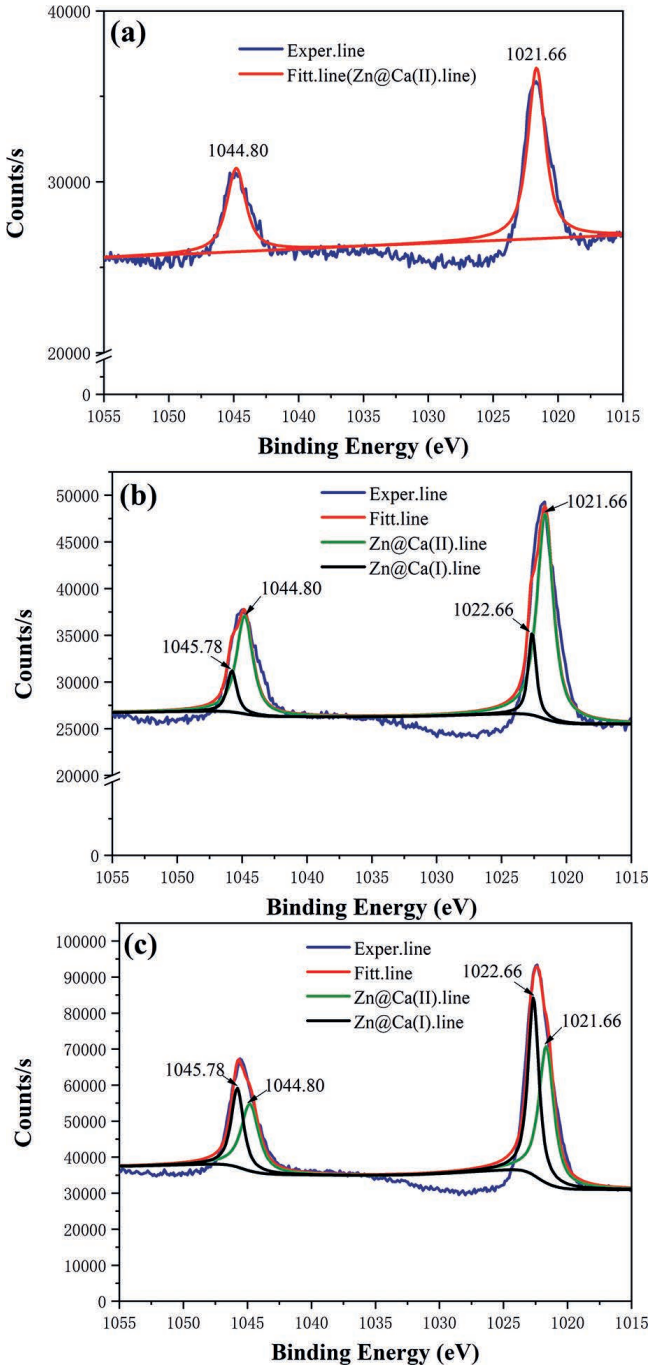

Fig. 6: The separated X-ray photoelectron spectroscopy of Zn 2p in ZnHA (a) Zn5-HA, (b) Zn10-HA, (c) Zn20-HA.

amorphous formation process and the transformation of the morphology. In the future, we shall continue to study the influence of Zn^{2+} ions occupying different Ca sites on the physical, chemical and biological properties of ZnHA.

IV. Conclusions

Zn-substituted nano-hydroxyapatite can be obtained with an aqueous precipitation method. With the increasing Zn^{2+} content, the crystallinity of ZnHA decreased and morphology of ZnHA powder changed gradually. Zn^{2+} ions inhibit the nucleation and growth of apatite, which is caused by the increase in lattice distortion energy. With low Zn addition (0 – 5 mol% Zn), ZnHA maintains the

same crystal structure of HA and nano-needle morphology, as Zn^{2+} ions occupy merely Ca(II) sites of the HA lattice. With a higher Zn^{2+} addition (10 – 20 mol% Zn), Zn-HA transforms into an amorphous state with nanosphere morphology, with Zn^{2+} ions occupying both Ca(I) and Ca(II) sites. As a result, the change in the morphology and crystal structure of ZnHA can be mainly attributed to the Zn^{2+} occupying Ca(I) sites in the HA lattice.

Acknowledgement

This research was funded by the International Science and Technology Cooperation Programme (2018YFE0194100), the Priority Academic Programme Development of Jiangsu Higher Education Institutions and the Funding of Jiangsu Innovation Programme for Graduate Education (KYLX15_0307).

References

1 Fox, K., Tran, P.A., Tran, N.: Recent advances in research applications of nanophase hydroxyapatite, *Chem. Phys. Chem.,* **13**, 2495 – 2506, (2012).

2 Zhang, Y.G., Zhu, Y.J., Chen, F.: Novel interconnected nanochannel hydroxyapatite ceramics: synthesis, microstructure, and permeability, *Ceram. Int.,* **43**, 5403 – 5411, (2017).

3 Dorozhkin, S.V.: Calcium orthophosphates in nature, biology and medicine, *Materials*, **2**, 399 – 498, (2009).

4 Bulut, B., Erkmen, Z.E., Kayali, E.S.: Biocompatibility of hydroxyapatite-alumina and hydroxyapatite-zirconia composites including commercial inert glass (CIG) as a ternary component, *J. Ceram. Sci. Tech.*, **7**, 263 – 276, (2016).

5 Greish, Y.E., Kenawy, S.H., Habib, S.I., Moussa, T.A., Shalaby, H.A., El Deftar, M.: Development of novel ZnO-doped hydroxyapatite polycarboxylate dental cement, *J. Ceram. Sci. Tech.*, **2**, 227 – 236, (2011).

6 Mehdi, R., Mohammadhossein, F., Omid, S., Lobat, T., Daryoosh, V.: Biodegradable magnesium bone implants coated with a novel bioceramic nanocomposite, *Materials,* **13**, 1315 – 1330, (2020).

7 Lowry, N., Brolly, M., Han, Y., McKillop, S., Meenan, B.J., Boyd, A.R.: Synthesis and characterisation of nanophase hydroxyapatite co-substituted with strontium and zinc, *Ceram. Int.,* **44**, 7761 – 7770, (2018).

8 Kumar, G.S., Thamizhavel, A., Yokogawa Y., Narayana Kalkura, S., Girija, E.K.: Synthesis, characterization and *in vitro* studies of zinc and carbonate co-substituted nano-hydroxyapatite for biomedical applications, *Mater. Chem. Phys.,* **134**, 1127 – 1135, (2012).

9 Tank, K.P., Chudasama, K.S., Thaker, V.S., Mihi, J.J.: Pure and zinc doped nano-hydroxyapatite: synthesis, characterization, antimicrobial and hemolytic studies, *J. Cryst. Growth,* **401**, 474 – 479, (2014).

10 Iyengar, G.V., Kollmer, W.E., Brown, H.J.M.: The elemental composition of human tissues and body Fluids: a compilation of values for adults., *Int. J. Environ. Res.,* **58**, 151 – 152 (1978).

11 Yuan, H.P., Fernandes, H., Habibovic, P., *et al.*: 'Smart' biomaterials and osteoinductivity, *Nat. Rev. Rheumatol.*, **7**, 1 – 1, (2011).

12 Webster, T.J., Ergun, C., Doremus, R.H., Rena, B.: Hydroxylapatite with substituted magnesium, zinc, cadmium, and yttrium. II. mechanisms of osteoblast adhesion, *J. Biomed. Mater. Res. A*, **59**, 312 – 317, (2002).

13 Santos, M.H., Valerio, P., Goes, A.M., Leite, M.F., Heneine, L.G.D., Mansur, H.S.: Biocompatibility evaluation of hydroxyapatite/collagen nanocomposites doped with Zn^{2+}, *Biomed. Mater.,* **2**, 135 – 141, (2007).

14 Bandyopadhyay, A., Bernard, S., Xue, W.C., Bose, S.: Calcium phosphate-based resorbable Ceramics: influence of MgO, ZnO, and SiO_2 dopants, *J. Am. Ceram. Soc.*, **89**, 2675 – 2688, (2006).

15 Otsuka M., Ohshita Y., Marunaka S., Matsuda Y., Ito A., Ichinose N., Otsuka K., Higuchi W.I.: Effect of controlled zinc release on bone mineral density from injectable Zn-containing -tricalcium phosphate suspension in zinc-deficient diseased rats, *J. Biomed. Mater. Res.,* **69A**, 552 – 560, (2004).

16 Matsunaga, K., Inamori, H., Murata, H.: Theoretical trend of ion exchange ability with divalent cations in hydroxyapatite, *Phys. Rev. B.*, **78**, 094 – 101, (2008).

17 Byeon, I.S., Hwang, I.J., Choe, H.C., Brantley, W.A.: Electrochemically-coated hydroxyapatite films on nanotubular ti-nb alloys prepared in solutions containing ca, P, and zn ions, *Thin Solid Films,* **620**, 132 – 138, (2016).

18 Montoya-Cisneros, K.L., Rendón-Ángeles, J.C., Matamoros-Veloza, Z., Yanagisawa, K.: Rapid synthesis and characterization of zn substituted hydroxyapatite nanoparticles via a microwave-assisted hydrothermal method, *Mater, Lett.,* **195**, 5 – 9, (2017).

19 Lyasnikova, A.V., Markelova, O.A., Lyasnikov, V.N., Dudareva, O.A.: Biocomposite plasma-sprayed coatings based on zinc-substituted hydroxyapatite: structure, properties, and prospects of application, *Mech. Compos. Mater.,* **51**, 1 – 4, (2016).

20 Koroleva, M.Y., Fadeeva, E.Y., Shkinev, V.M., Katasonova, O.N., Yurtov, E.V.: Hydroxyapatite nanoparticle prepared by controlled precipitation from aqueous phase, *Russ. J. Inorg.* Chem., **61**, 674 – 680, (2016).

21 Kaygili, O., Keser, S.V.: Sol-gel synthesis and characterization of Sr/Mg, Mg/Zn and Sr/Zn co-doped hydroxyapatites, *Mater. Lett.,* **141**, 161 – 164, (2015).

22 Ren, F., Xin, R., Ge, X., Leng, Y.: Characterization and structural analysis of zinc-substituted hydroxyapatites, *Acta Biomater.,* **5**, 3141 – 3149, (2009).

23 Tang, Y., Chappell, H.F., Dove, M.T., Reeder, R.J., Lee, Y.J.: Zinc incorporation into hydroxylapatite, *Biomaterials,* **30**, 2864 – 2872, (2009).

24 Kanazawa, T., Monma, H.: Amorphous calcium phosphate, *Inorg. Mater.*, **1975**, 187 – 191, (1975).

25 Blumenthal, N.C., Posner, A.S, Holmes, J.M.: Effect of preparation conditions on the properties and transformation of amorphous calcium phosphate, *Mater. Res. Bull.,* **7**, 1181 – 1189, (1972).

26 Kumar, G.S., Thamizhavel, A., Yokogawa, Y., Kalkura, S.N., Girija, E.K.: Synthesis, characterization and invitro, studies of zinc and carbonate co-substituted nano-hydroxyapatite for biomedical applications, *Mater. Chem. Phys.,* **134**, 1127 – 1135, (2012).

27 Moulder, J.F., Stickle, W.F., Sobol, P.E., Bomben, K.D.: Handbook of X-ray photoelectron spectroscopy. 1st ed. Perkin-Elmer Corporation, Minnesota, 1992.

28 Lala, S., Ghosh, M., Das, P.K., Das, D., Kar, T., Pradhan, S.K.: Structural and microstructural interpretations of Zn-doped biocompatible bone-like carbonated hydroxyapatite synthesized by mechanical alloying, *J. Appl. Crystallogr.,* **48**, 138 – 148, (2015).

29 Guo, D.G., Hao, Y.Z., Li, H.Y., Fang, C.Q., Sun, L.J., Zhu, H., Wang, J., Huang, X.F., Ni, P.F., Xu, K.W.: Influences of sr dose on the crystal structure parameters and sr distributions of Sr-incorporated hydroxyapatite, *J. Biomed. Mater. Res. B,* **101**, 1275 – 1283, (2014).